APL Photonics

RESEARCH ARTICLE | JANUARY 06 2025

Scanless laser waveform measurement in the near-infrared

Tran-Chau Truong ; Yangyang Liu; Dipendra Khatri ; Yuxuan Zhang ; Bonggu Shim ; Michael Chini

APL Photonics 10, 016101 (2025)
https://doi.org/10.1063/5.0239294
CHORUS

Scanless laser waveform measurement in the near-infrared

Cite as: APL Photon. 10, 016101 (2025); doi: 10.1063/5.0239294
Submitted: 18 September 2024 • Accepted: 19 December 2024 •
Published Online: 6 January 2025

Tran-Chau Truong,[1,2] Yangyang Liu,[1,3] Dipendra Khatri,[1] Yuxuan Zhang,[4] Bonggu Shim,[4] and Michael Chini[1,2,5,a)]

AFFILIATIONS

[1] Department of Physics, University of Central Florida, Orlando, Florida 32816, USA
[2] Department of Physics, The Ohio State University, Columbus, Ohio 43210, USA
[3] School of Optical and Electronic Information, Huazhong University of Science and Technology, Wuhan 430074, China
[4] Department of Physics, Applied Physics and Astronomy, Binghamton University, Binghamton, New York 13902, USA
[5] CREOL, the College of Optics and Photonics, University of Central Florida, Orlando, Florida 32816, USA

[a)] **Author to whom correspondence should be addressed:** chini.4@osu.edu

ABSTRACT

Field-resolved measurements of few-cycle laser waveforms allow access to ultrafast electron dynamics in light–matter interactions and are key to future lightwave electronics. Recently, sub-cycle gating based on nonlinear excitation in active pixel sensors has allowed the first single-shot measurements of mid-infrared optical fields. Extending the techniques to shorter wavelengths, however, is not feasible using silicon-based detectors with bandgaps in the near-infrared. Here, we demonstrate an all-optical sampling technique for near-infrared laser fields, wherein an intense fundamental field generates a sub-cycle gate through nonlinear excitation of a wide-bandgap crystal, in this case, ZnO, which can sample the electric field of a weak perturbing pulse. By using a crossed-beam geometry, the temporal evolution of the perturbing field is mapped onto a transverse spatial axis of the nonlinear medium, and the waveform is captured in a single measurement of the spatially resolved fluorescence emission from the crystal. The technique is demonstrated through field-resolved measurements of the field reshaping during nonlinear propagation in the ZnO detection crystal.

I. INTRODUCTION

The development of ultrafast laser technology has provided powerful tools for measuring and controlling strong-field light–matter interactions with unprecedented time resolution. In particular, the emergence of intense, few-cycle laser waveforms with well-controlled electric fields has allowed the transition of measurements from the perturbative regime, where the intensity envelope controls the evolution of nonlinear processes, to the strong-field regime, where dynamics are driven by sub-cycle electric fields on the attosecond time scale. With the recent development of advanced, field-resolved metrology tools,[1–10] it has been shown that rich dynamics of optical excitation, material polarization, and light–matter energy transfer are imprinted on the light pulse itself and can be extracted from minute changes in the measured electric field.[11] Now, field-resolved techniques are providing novel approaches to spectroscopy[12,13] and microscopy[14–16] and promise major advances in diverse fields ranging from nanophotonics to therapeutic medicine.

The primary requirement for sampling an arbitrary laser field is a fast temporal gate, whose duration is less than half-cycle of the measured electric field. This can be implemented by using a few-cycle sampling pulse with a shorter wavelength than that of the field to be measured. The full characterization of terahertz (THz) fields was first demonstrated in this manner by electro-optic sampling[1] with near-infrared probe pulses, and the technique was later adapted to allow sampling of mid- and near-infrared fields through the use of few-cycle UV probes.[4,17] Further pushing waveform sampling into the visible spectrum is more challenging, as it requires sub-femtosecond gate fields to resolve the field oscillations. The generation of isolated attosecond pulses via high-order harmonic generation (HHG)[18,19] provided such a short gate for direct waveform measurement throughout the near-infrared and visible spectral regions by attosecond streaking.[2,20]

Advances in our understanding of strong-field processes have led to novel techniques through which a few-cycle field can be used to sample itself, analogous to widely used pulse measurement techniques based on perturbative nonlinear optics.[21,22] These techniques all satisfy the requirement of a sub-cycle gate, such as sub-cycle electron trajectories in HHG,[3,5] tunneling ionization in gases,[7] and strong-field excitation in solids.[8–10,23–26] In the last decade, numerous field sampling techniques have been demonstrated to be capable of providing complete waveform measurements across the electromagnetic spectrum from the mid-infrared (mid-IR) to ultraviolet[4,15,26–31] and with sensitivity down to the nanojoule level.[10] However, unlike conventional pulse characterization methods, these sampling techniques have all been based on scanning geometry measurements, which require identical laser pulses with excellent energy and carrier-envelope phase stability over extended measurement periods. Recently, a novel approach based on the nonlinear excitation of a Si-based CMOS image sensor, combined with time-to-space mapping in a crossed-beam geometry, allowed for the first single-shot field sampling measurements in the mid-IR.[28] However, the reliance on nonlinear interactions in silicon, with an indirect bandgap of ~1 eV, does not allow sampling measurements in the near-infrared or shorter wavelength regions.

In this work, we use multiphoton excitation, driven by few-cycle near-infrared pulses in a wide-bandgap ZnO crystal, and spatially resolved measurements of the resulting fluorescence emission to demonstrate sampling of near-infrared laser waveforms in a scanning-free geometry. As in our previous work, the sub-cycle gate is generated by multiphoton excitation in ZnO (3.3 eV bandgap), allowing the measurement of a spectrum of above 950 nm.[9] However, here, the scanning-free measurement geometry is implemented by introducing a small crossing angle between the intense fundamental and weak perturbing pulses, which maps the time delay axis onto a transverse spatial axis in the surface plane of the crystal. The spatially resolved fluorescence emission, obtained by imaging the spatially and spectrally filtered band fluorescence emission onto a camera sensor, encodes the laser electric field. We further show that a single measurement encodes two distinct waveforms—at the entrance and exit planes of the ZnO crystal—from which we can extract information about the nonlinear reshaping of the laser during propagation in the crystal. This technique provides a unique platform for waveform characterization and field-resolved spectroscopy in the near-infrared.

II. EXPERIMENTAL SETUP AND FIELD SAMPLING

The single-shot waveform measurement is an adaptation of the TIPTOE (tunneling ionization with a perturbation for the time-domain observation of an electric field) technique.[7] In TIPTOE, tunneling or multiphoton ionization in gases, driven by an intense few-cycle "fundamental" field, was used as the sub-cycle temporal gate for sampling the electric field of a weaker "perturbing" pulse. The coherent addition of the fundamental and perturbation pulses leads to a delay-dependent modulation of the ionization probability, which could be directed by measuring the ionization yield between two electrodes. Finally, the laser waveform is sampled by measuring the ionization yield while varying the time delay between the two pulses. Later, it was shown that tunneling and multiphoton excitation in a solid could likewise be used to produce a sub-cycle gate[9] and that the waveform was similarly encoded in the intensity of the band fluorescence emitted from a crystal exposed to the combined fundamental and perturbing fields. Following this, the solid-state TIPTOE was adapted to a single-shot geometry,[28] using a Si-based CMOS image sensor as both the nonlinear medium and the detector, which allows the waveform measurement for mid-IR and longer wavelengths.

Extending the waveform measurement into near-IR can, in principle, be achieved by using solids with larger bandgaps. Our previous work[9] shows the potential of measuring near-infrared laser fields using nonlinear excitation and band fluorescence emission in ZnO. In this case, the sub-cycle temporal gate is generated via multiphoton excitation of electrons from the valence band to the conduction band, and the subsequent radiative relaxation leads to the emission of incoherent band fluorescence on sub-nanosecond time scales. This multiphoton excitation is modulated by the coherent addition of the perturbation pulse, depending on the time delay between the two fields, and the perturbing pulse waveform is thereby encoded in the delay-resolved fluorescence intensity.

We adapt the solid-state TIPTOE technique, using multiphoton excitation in ZnO as the sub-cycle gate, to a scanning-free geometry by introducing a small crossing angle between the fundamental and perturbation fields and by using an imaging setup to spatially resolve the modulated fluorescence signal. The experimental setup is shown in Fig. 1. Here, the incoming beam is separated into fundamental and perturbative arms of a Mach–Zehnder-type interferometer by a pair of CaF_2 wedges working as a beam splitter. In TIPTOE, the intensity of the fundamental pulse should be ~1000 times stronger than that of the perturbation, and so the perturbation pulse is further attenuated by a variable neutral density filter. An equivalent amount of glass is included in the fundamental arm to balance the dispersion. The two beams are then focused on a 0.5 mm thick, c-cut ZnO crystal by a cylindrical mirror (f = 100 mm). A small crossing angle of ~3° is used to map the time delay axis onto a transverse spatial axis of the crystal, which provides sufficient temporal resolution to resolve the electric field waveform as discussed in Note 1 of the supplementary material. Finally, the band fluorescence emission is collected by imaging the signal onto a Si-based camera using a lens of 50 mm focal length and a narrow-linewidth bandpass filter to select the fluorescence emission line. To avoid contributions from the fundamental and perturbation pulses, as well as their third harmonics, the optical axis of the imaging setup is oriented at an angle of ~15° with respect to the plane of propagation. The pure band fluorescence signal is confirmed by the insertion of a rotatable polarizer in the imaging setup, which shows that the measured light is unpolarized.

In our experiment, the few-cycle laser pulses are derived from multidimensional solitary states generated in an N_2O-filled hollow-core fiber,[32–35] which are compressed using bulk glass to a duration of ~13 fs at a central wavelength of 1170 nm.[34] The laser pulses with 400 μJ pulse energy, 280 fs pulse duration, and 1.03 μm center wavelength from a commercial Yb:KGW amplifier (Light Conversion PHAROS) are sent through an N_2O gas-filled hollow-core capillary fiber (1.4 m length and 400 μm inner diameter) for spectral broadening. The rotational Raman-enhanced self-phase modulation results in a red-shifted supercontinuum spectrum, from which the spectral region between ~1000 and 1500 nm is selected using dichroic mirrors. The rotational nonlinearity of molecular gases imposes a negative chirp on the broadened laser pulse, which allows

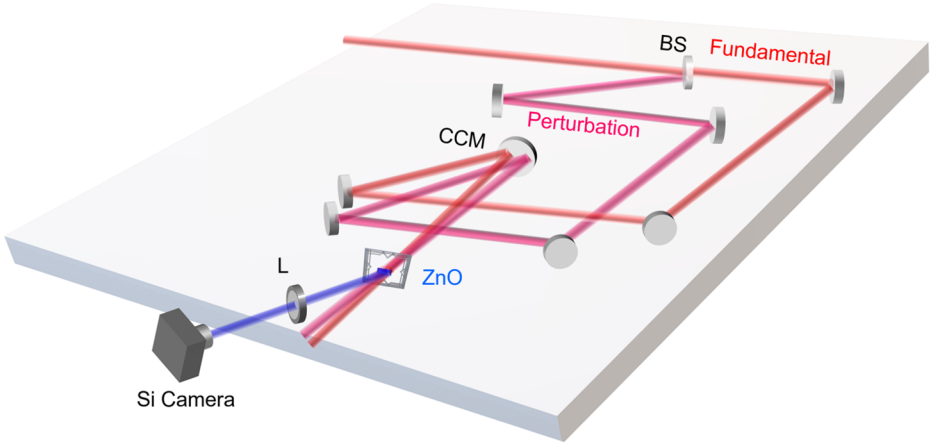

FIG. 1. Experimental setup of single-image optical waveform measurement. BS: beam splitter, CCM: concave cylindrical mirror, and L: plano–convex lens.

for pulse compression by propagation in normally dispersive bulk materials,[32,33] in this case, CaF_2 and fused silica windows. A detailed discussion about the laser source is provided in Note 2 of the supplementary material. Due to spectral narrowing at high repetition rates,[36] we restricted the repetition rate of the laser to 0.25 kHz for all measurements. We also note that the carrier-envelope phase (CEP) of the laser was not stabilized during the experiments, and therefore, the measurements reflect the relative CEP between the fundamental and perturbing pulses, rather than the absolute CEP of the perturbing pulse. The pulse characterization was implemented by our technique and a single-shot home-built SHG FROG.

The band fluorescence images spatial lineouts for fundamental-only excitation and with the addition of the perturbating pulse are shown in Fig. 2. All recorded images were averaged over 20 000 laser shots to have a sufficient signal-to-noise ratio. As expected, the band fluorescence emission is observed with the fundamental pulse and from the combination of the fundamental and perturbing pulses, but not from the weak perturbing pulse alone. The excitation rate S, and thus the band fluorescence emission intensity, depends on the laser intensity and the multiphoton number q as $S \propto I^q$. By measuring the band fluorescence intensity as a function of the fundamental intensity, the effective multiphoton scaling parameter q can be calculated, which is found to be ~3.25 for our experimental conditions. The addition of the perturbing pulse imprints a modulation on the multiphoton excitation probability, which enhances and suppresses the conduction band population, depending on the time delay between the two fields. As a result, the spatially resolved band fluorescence emission encodes the waveform of the few-cycle pulses.

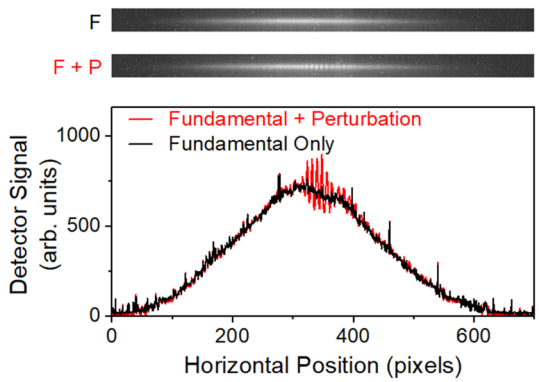

FIG. 2. Waveform extraction. Top: Single-image measurements of band fluorescence signals with fundamental pulse only (F) and with both fundamental and perturbing pulses (F + P). Bottom: Lineouts show the modulation of band fluorescence signal induced by the perturbing pulses.

The extraction of the laser waveform from the fluorescence image follows the same process described in Ref. 28. First, the modulation amplitude imposed by the perturbing field is obtained by subtracting the spatially resolved band fluorescence intensity obtained with the fundamental pulse only from the modulated fluorescence intensity obtained with both fields. Converting this modulation amplitude to an electric field further requires a normalization process, in which the spatial dependence of the excitation probability, which is caused by the spatial intensity variation of the fundamental laser pulse, must be accounted for. This spatial effect can be straightforwardly removed by a simple normalization process, in which the electric field is calculated according to $E = \frac{S_{F+P} - S_F}{S_F^n}$, where S_{F+P} and S_F are the fluorescence signals for fundamental plus perturbation and for fundamental only, as shown in Fig. 2; and $n = \frac{2q-1}{2q}$ is a scaling factor for normalization calculated from the value of effective multiphoton scaling parameter q. The value of q depends primarily on the bandgap ΔE_{gap} of the crystal and the central frequency ω_L of the laser pulse and can be approximated as $q \approx \frac{\Delta E_{gap}}{\omega_L}$ without significant loss of accuracy in the measured waveform.[28] The mapping of time delay to the horizontal spatial axis of the pixelated detector is estimated from the measurement geometry and confirmed through a calibration measurement in which the time delay between the fundamental and perturbation beams is shifted using a manual translation stage in the fundamental arm, which yields a linear space-to-time mapping coefficient of 0.48 fs/pixel.

The time-domain waveform obtained from the single-image TIPTOE measurement, along with its field envelope and the pulse envelope retrieved from the second harmonic generation frequency-resolved optical gating technique (SHG FROG), are shown in Fig. 3(a). While the SHG FROG inherently has time-axis ambiguity,

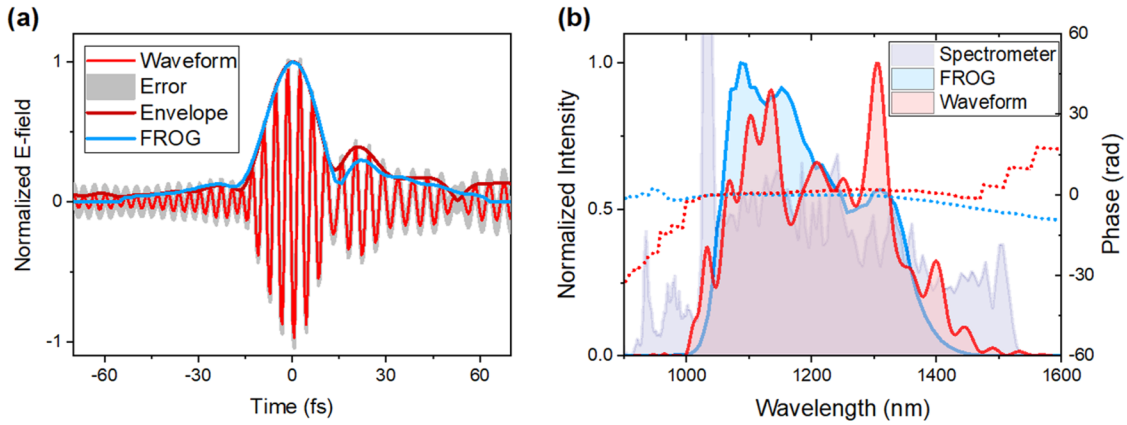

FIG. 3. Pulse characterization. (a) Measured optical waveform (red) after subtraction of fundamental signal only and doing normalization process with its standard deviation (gray area) and optical pulse envelope retrieved from FROG technique (blue) under similar conditions. (b) Measured spectra from a spectrometer (purple); calculated spectral intensities (solid line) and spectral phases (dashed line) from two techniques.

our measurement allows for the determination of absolute time due to the directional information provided by the camera and the imaging apparatus. We find that the TIPTOE and FROG measurements yield nearly identical envelopes with the same pulse duration (intensity full-width at half-maximum) of 12.5 fs. Furthermore, the spectral intensities and phases, obtained from the Fourier transform of the TIPTOE waveform and the FROG retrieval, are in excellent agreement with one another, as shown in Fig. 3(b). There are, however, discrepancies between the spectra obtained from the time-domain measurements and the measured spectrum of the pulses after the dichroic mirrors, which we attribute to strong spectral phase variation near the edges of the mirror reflectivity windows, as well as the inability to compress the full spectrum using bulk materials. These effects will lead to spectral components that are delayed in time with respect to the main pulse and that are not captured within the finite time window of the FROG and single-image TIPTOE measurements.

As indicated above, the TIPTOE measurement was performed using a few-cycle laser source with unstable CEP. In principle, the absolute CEP measurement of the perturbing pulse could be implemented by setting the fundamental pulse's CEP equal to zero, for example, by adding a second-harmonic waveform to the perturbation arm of the interferometer[7,28] or by simultaneous measurement of the TIPTOE waveform and the above-threshold ionization signal or high-order harmonic spectrum.[37] In general, these techniques all require sub-two-cycle waveforms to unambiguously determine the absolute CEP, and therefore, they could not be realized with our laser source. In addition, while the experimental waveforms were obtained from a single image of the band fluorescence emission, a true single-shot measurement could not be realized. We believe that it may be possible to overcome this restriction in the future: We use an optical imaging setup with an estimated collection efficiency below 0.15% for band emission emitted in a 4π solid angle and operate at peak intensities below both the multiphoton lasing threshold[38] and the damage threshold of ZnO. Increasing the laser peak power, therefore, would provide a dramatic signal enhancement due to both the nonlinearity of the excitation process and the transition to directed laser emission, while a well-designed imaging system could provide substantial improvements to the photon collection efficiency.

III. NONLINEAR PROPAGATION IN ZNO

While the above measurements were based on fluorescence emission from the entrance plane of the ZnO crystal, the finite thickness of the crystal allows us also to record the reshaping of the optical waveform due to linear and nonlinear propagation effects. In these experiments, the vertical inclination of the optical imaging axis allowed us to simultaneously record distinct band fluorescence signals from the entrance and exit surfaces of the crystal in a single image. As shown in Fig. 4, the TIPTOE waveform at the exit surface exhibits a noticeable phase shift and a reduction in amplitude. Furthermore, the spectrum of the laser is significantly reshaped, most evident from an overall spectral broadening and the formation of a new spectral peak on the long-wavelength side of the spectrum.

To better understand the source of these phenomena, we compare the measured waveform and spectrum to simulations based on numerical solutions to the carrier-resolved unidirectional pulse propagation equations (UPPEs), including the linear, nonlinear, and plasma responses of the medium.[39,40] A table of parameters used in the UPPE simulation is provided in Note 3 of the supplementary material. Since it is computationally expensive to perform fully 3D simulations considering spatial ellipticity, we perform spatiotemporal simulations assuming a circular beam with the input intensities used for the experiment but the radius for the minor axis. However, for spatial cylindrical beams, the critical power for self-focusing is larger than that for circular beams, resulting in the decrease in the effective optical Kerr nonlinearity (e.g., self-focusing).[41–43] Therefore, we empirically decrease n_2 from the known value (5×10^{-19} m^2/W)[44] to match the experiment. In our simulations, we use the full Keldysh model[45] for plasma generation, which incorporates both multiphoton and tunneling ionization. Although collisional ionization is considered, its effect is not significant for our experimental parameters. We carry out simulations in the

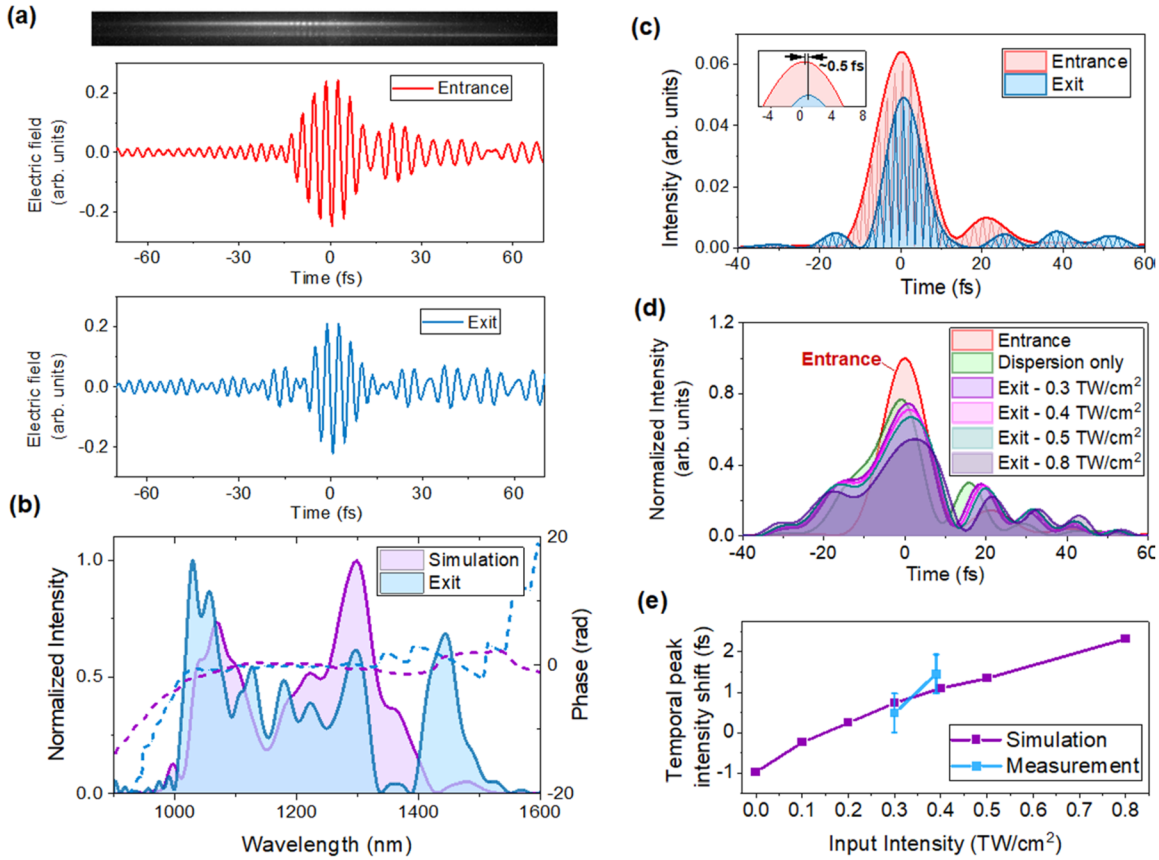

FIG. 4. Pulse propagation in a ZnO crystal. (a) Single image showing two sets of band fluorescence modulations corresponding to the entrance (top) and exit (bottom) planes of the ZnO crystal, and calculated waveforms from the entrance (red) and exit (blue); (b) calculated (blue) and simulated (purple) spectrum (solid lines) and spectral phase (dotted lines) at the exit of ZnO; (c) the temporal intensity of laser pulses at the entrance (red) and exit (blue) of a ZnO crystal; (d) simulated output temporal intensities at the exit of ZnO with different input intensities. The output amplitudes are scaled with the normalized input intensity at the entrance; and (e) output temporal peak intensity shift compared to the entrance from measurement (blue) and simulation (purple).

moving frame with the group velocity of the center wavelength (i.e., 1170 nm) in ZnO. The best agreement with experiments is obtained for the propagation of pulses with $n_2 = 2.5 \times 10^{-19}$ m^2/W and an incident intensity of 0.3 TW/cm^2 through a ZnO thickness of 0.5 mm, as shown in Fig. 4(b). In both measured and simulated data, the spectral phase is flat across the spectrum, and there is large spectral broadening, in particular, at long wavelengths. We further investigate the sources of temporal reshaping of the pulse during propagation. As shown in Fig. 4(c), the experiments reveal a temporal shift of the peak of the laser pulse by ~0.5 fs accompanied by a reduction in the amplitude. The simulation results for different input intensities show that the presence of dispersion alone causes the opposite temporal shift, which is toward the leading edge of the pulse [green line in Fig. 4(d)], although the output intensity is decreased due to dispersion. However, the temporal peak intensity is shifted toward the trailing edge of the pulse, and the intensity is reduced more when including the effects of nonlinear propagation and plasma generation. As shown in Fig. 4(e), the observed temporal shifts in the measurement are consistent with a simulated input peak intensity of ~0.3 and ~0.4 TW/cm^2. This shows the potential aspect of this technique for probing the nonlinear propagation in materials.

IV. CONCLUSION

In conclusion, we demonstrate a simple, all-optical method for scanning-free measurements of near-infrared electric fields using multiphoton-induced fluorescence as the nonlinear signal and demonstrate the technique through single-image of few-cycle pulses centered near 1200 nm. The validity is confirmed through comparison with independent measurements of the field envelope using FROG. Furthermore, we show that the technique using ZnO crystal provides a versatile tool not only for complete temporal characterization of few-cycle laser pulses with a spectrum of above 950 nm but also for detecting the changes to optical fields through field-resolved spectroscopy.

The demonstrations of TIPTOE measurements with a crossed beam geometry using both electro-optic[26] and fluorescence imaging

detection (this work) suggest a near-universal approach to single-image, and in some cases single-shot, measurement of optical electric fields. To fully realize these capabilities, further investigations into appropriate detection methods for different wavelength ranges are needed. Our preliminary investigations have identified ZnO as a good candidate for near-infrared detection due to its reasonably wide bandgap and high fluorescence yield, as well as the commercial availability of high-quality bulk crystals. While other semiconductors with higher fluorescence yield (e.g., thin films of semiconductor quantum dots) may provide increased signal levels for some applications, such materials tend to suffer from issues such as photobleaching and color center formation. On the other hand, bulk crystals with higher bandgaps (e.g., AlGaN and CVD-grown diamond) may provide enhanced detection bandwidth, but they have very low fluorescence yields. Further developments, such as the use of arrays of solar-blind UV photodetectors[46] or improvements to the optical imaging system to enable the efficient detection of low-flux fluorescence signals from wide-bandgap insulators or gas-phase "sheets," could enable the extension of single-shot field measurements of few-cycle pulses extending further into the short-wavelength regions of the electromagnetic spectrum.

SUPPLEMENTARY MATERIAL

See the supplementary material for the information on the laser source, time window and time resolution of the scanless waveform measurement, and parameters for UPPE simulation.

ACKNOWLEDGMENTS

This material is based primarily on research supported by the Department of Energy (DOE), Office of Science, Basic Energy Sciences (BES), under Award No. DE-SC0019291 (T.-C.T. and M.C.). Y.L. was supported by the Air Force Office of Scientific Research under Award No. FA9550-20-1-0284. D.K. was partially supported by the Department of Energy, Office of Science, Fusion Energy Sciences (FES), under Award No. DE-SC0022540. Y.Z. and B.S. are supported by the National Science Foundation (NSF) under Award Nos. PHY-2010365 and PHY-2409415 and IEEC of Binghamton University.

AUTHOR DECLARATIONS

Conflict of Interest

The authors have no conflicts to disclose.

Author Contributions

Tran-Chau Truong: Investigation (equal); Methodology (equal); Validation (equal); Visualization (equal); Writing – original draft (equal); Writing – review & editing (equal). **Yangyang Liu**: Investigation (equal); Methodology (equal); Visualization (equal); Writing – review & editing (equal). **Dipendra Khatri**: Investigation (equal); Writing – review & editing (equal). **Yuxuan Zhang**: Software (equal); Writing – review & editing (equal). **Bonggu Shim**: Software (equal); Supervision (equal); Writing – review & editing (equal). **Michael Chini**: Conceptualization (lead); Methodology (equal); Supervision (lead); Writing – review & editing (equal).

DATA AVAILABILITY

Data underlying the results presented in this paper are not publicly available at this time but may be obtained from the authors upon reasonable request.

REFERENCES

[1] Q. Wu and X. C. Zhang, "Free-space electro-optic sampling of terahertz beams," Appl. Phys. Lett. **67**, 3523–3525 (1995).
[2] E. Goulielmakis, M. Uiberacker, R. Kienberger *et al.*, "Direct measurement of light waves," Science **305**, 1267–1269 (2004).
[3] K. T. Kim, C. Zhang, A. D. Shiner *et al.*, "Petahertz optical oscilloscope," Nat. Photonics **7**, 958–962 (2013).
[4] S. Keiber, S. Sederberg, A. Schwarz *et al.*, "Electro-optic sampling of near-infrared waveforms," Nat. Photonics **10**, 159–162 (2016).
[5] A. S. Wyatt, T. Witting, A. Schiavi *et al.*, "Attosecond sampling of arbitrary optical waveforms," Optica **3**, 303–310 (2016).
[6] T. Paasch-Colberg, S. Y. Kruchinin, Ö. Sağlam *et al.*, "Sub-cycle optical control of current in a semiconductor: From the multiphoton to the tunneling regime," Optica **3**, 1358–1361 (2016).
[7] S. B. Park, K. Kim, W. Cho *et al.*, "Direct sampling of a light wave in air," Optica **5**, 402–408 (2018).
[8] A. Korobenko, K. Johnston, M. Kubullek *et al.*, "Femtosecond streaking in ambient air," Optica **7**, 1372–1376 (2020).
[9] Y. Liu, S. Gholam-Mirzaei, J. E. Beetar *et al.*, "All-optical sampling of few-cycle infrared pulses using tunneling in a solid," Photonics Res. **9**, 929–936 (2021).
[10] M. R. Bionta, F. Ritzkowsky, M. Turchetti *et al.*, "On-chip sampling of optical fields with attosecond resolution," Nat. Photonics **15**, 456–460 (2021).
[11] A. Sommer, E. M. Bothschafter, S. A. Sato *et al.*, "Attosecond nonlinear polarization and light–matter energy transfer in solids," Nature **534**, 86–90 (2016).
[12] I. Pupeza, M. Huber, M. Trubetskov *et al.*, "Field-resolved infrared spectroscopy of biological systems," Nature **577**, 52–59 (2020).
[13] A. Srivastava, A. Herbst, M. M. Bidhendi *et al.*, "Near-petahertz fieldoscopy of liquid," Nat. Photonics **18**, 1320–1326 (2024).
[14] M. Mamaikin, Y.-L. Li, E. Ridente *et al.*, "Electric-field-resolved near-infrared microscopy," Optica **9**, 616–622 (2022).
[15] J. Blöchl, J. Schötz, A. Maliakkal *et al.*, "Spatiotemporal sampling of near-petahertz vortex fields," Optica **9**, 755–761 (2022).
[16] D. Hui, H. Alqattan, M. Sennary *et al.*, "Attosecond electron microscopy and diffraction," Sci. Adv. **10**, eadp5805 (2024).
[17] E. Ridente, M. Mamaikin, N. Altwaijry *et al.*, "Electro-optic characterization of synthesized infrared-visible light fields," Nat. Commun. **13**, 1111 (2022).
[18] M. Hentschel, R. Kienberger, C. Spielmann *et al.*, "Attosecond metrology," Nature **414**, 509–513 (2001).
[19] M. Chini, K. Zhao, and Z. Chang, "The generation, characterization and applications of broadband isolated attosecond pulses," Nat. Photonics **8**, 178–186 (2014).
[20] H. Mashiko, M. J. Bell, A. R. Beck *et al.*, "Tunable frequency-controlled isolated attosecond pulses characterized by either 750 nm or 400 nm wavelength streak fields," Opt. Express **18**, 25887–25895 (2010).
[21] R. Trebino, K. W. DeLong, D. N. Fittinghoff *et al.*, "Measuring ultrashort laser pulses in the time-frequency domain using frequency-resolved optical gating," Rev. Sci. Instrum. **68**, 3277–3295 (1997).
[22] C. Iaconis and I. A. Walmsley, "Spectral phase interferometry for direct electric-field reconstruction of ultrashort optical pulses," Opt. Lett. **23**, 792–794 (1998).
[23] S. Sederberg, D. Zimin, S. Keiber *et al.*, "Attosecond optoelectronic field measurement in solids," Nat. Commun. **11**, 430 (2020).

[24]M. Kubullek, Z. Wang, K. von der Brelje *et al.*, "Single-shot carrier–envelope-phase measurement in ambient air," Optica **7**, 35–39 (2020).
[25]D. Zimin, M. Weidman, J. Schötz *et al.*, "Petahertz-scale nonlinear photoconductive sampling in air," Optica **8**, 586–590 (2021).
[26]D. Hui, H. Alqattan, S. Yamada *et al.*, "Attosecond electron motion control in dielectric," Nat. Photonics **16**, 33–37 (2022).
[27]W. Cho, S. I. Hwang, C. H. Nam *et al.*, "Temporal characterization of femtosecond laser pulses using tunneling ionization in the UV, visible, and mid-IR ranges," Sci. Rep. **9**, 16067 (2019).
[28]Y. Liu, J. E. Beetar, J. Nesper *et al.*, "Single-shot measurement of few-cycle optical waveforms on a chip," Nat. Photonics **16**, 109–112 (2022).
[29]T. J. Hammond, A. Korobenko, A. Y. Naumov *et al.*, "Near-field imaging for single-shot waveform measurements," J. Phys. B: At., Mol. Opt. Phys. **51**, 065603 (2018).
[30]Y. Luo, A. Martin-Jimenez, F. Neubrech *et al.*, "Synthesis and direct sampling of single-cycle light transients by electron tunneling in a nanodevice," ACS Photonics **10**, 2866–2873 (2023).
[31]F. Ritzkowsky, M. Yeung, E. Bebeti *et al.*, "On-chip petahertz electronics for single-shot phase detection," Nat. Commun. **15**, 10179 (2024).
[32]R. Safaei, G. Fan, O. Kwon *et al.*, "High-energy multidimensional solitary states in hollow-core fibres," Nat. Photonics **14**, 733–739 (2020).
[33]J. E. Beetar, M. Nrisimhamurty, T. C. Truong *et al.*, "Multioctave supercontinuum generation and frequency conversion based on rotational nonlinearity," Sci. Adv. **6**, eabb5375 (2020).
[34]T. C. Truong, J. E. Beetar, and M. Chini, "Light-field synthesizer based on multidimensional solitary states in hollow-core fibers," Opt. Lett. **48**, 2397–2400 (2023).
[35]T. C. Truong, C. Lantigua, Y. Zhang *et al.*, "Spectral broadening and pulse compression in molecular gas-filled hollow-core fibers," IEEE J. Sel. Top. Quantum Electron. **30**, 1–11 (2024).
[36]J. E. Beetar, M. Nrisimhamurty, T. C. Truong *et al.*, "Thermal effects in molecular gas-filled hollow-core fibers," Opt. Lett. **46**, 2437–2440 (2021).
[37]G. G. Paulus, F. Grasbon, H. Walther *et al.*, "Absolute-phase phenomena in photoionization with few-cycle laser pulses," Nature **414**, 182–184 (2001).
[38]M. Wille, C. Sturm, T. Michalsky *et al.*, "Carrier density driven lasing dynamics in ZnO nanowires," Nanotechnology **27**, 225702 (2016).
[39]R. I. Grynko, G. C. Nagar, and B. Shim, "Wavelength-scaled laser filamentation in solids and plasma-assisted subcycle light-bullet generation in the long-wavelength infrared," Phys. Rev. A **98**, 023844 (2018).
[40]A. Couairon, E. Brambilla, T. Corti *et al.*, "Practitioner's guide to laser pulse propagation models and simulation," Eur. Phys. J.: Spec. Top. **199**, 5–76 (2011).
[41]G. Fibich and B. Ilan, "Self-focusing of elliptic beams: An example of the failure of the aberrationless approximation," J. Opt. Soc. Am. B **17**, 1749 (2000).
[42]V. P. Kandidov and V. Yu. Fedorov, "Properties of self-focusing of elliptic beams," Quantum Electron. **34**, 1163 (2004).
[43]B. Shim, S. E. Schrauth, L. T. Vuong *et al.*, "Dynamics of elliptical beams in the anomalous group-velocity dispersion regime," Opt. Express **19**, 9139 (2011).
[44]R. Adair, L. L. Chase, and S. A. Payne, "Nonlinear refractive index of optical crystals," Phys. Rev. B **39**, 3337 (1989).
[45]L. V. Keldysh, "Ionization in the field of a strong electromagnetic wave," J. Exp. Theor. Phys. (U.S.S.R.) **47**, 1945 (1964).
[46]C. Lantigua, T.-C. Truong, C. Kincaid *et al.*, "TIPTOE laser waveform sampling with AlGaN photodiode for fast scanning measurements," in *CLEO* (Optica Publishing Group, 2024).